arXiv:astro-ph/0509087v1 5 Sep 2005

Metallicities, relative ages and kinematics of stellar populations in ω Centauri[1]

A. Sollima[1], E. Pancino[2], F. R. Ferraro[1], M. Bellazzini[2], O. Straniero[3] and L. Pasquini[4]

ABSTRACT

We present results of an extensive spectroscopic survey of Subgiant stars in the stellar system ω Centauri. Using infrared Ca II triplet lines, we derived metallicities and radial velocities for more than 250 stars belonging to different stellar populations of the system. We find that the most metal rich component, the anomalous Sub Giant Branch (SGB-a), has a metallicity of [Fe/H] $\sim$ -0.6 fully compatible with that determined along the anomalous Red Giant Branch (RGB-a). Our analysis suggests that the age of this component and of the other metal-intermediate ($-1.4 < [Fe/H] < -1.0$) stellar populations of the system are all comparable to that of the dominant metal poor population within 2 Gyr, regardless of any choice of helium abundance. These results impose severe constraints on the time-scale of the enrichment process of this stellar system, excluding the possibility of an extended star formation period. The radial velocity analysis of the entire sample demonstrates that only metal-intermediate populations are kinematically cooler than the others.

Subject headings: techniques: spectroscopic – stars: abundances – stars: evolution – stars: Population II – globular cluster: ω Cen

1. Introduction

The understanding of the origin and star formation history of the stellar system ω Centauri (NGC 5139), the most massive and luminous globular cluster of the Milky Way

[1]Dipartimento di Astronomia, Università di Bologna, via Ranzani 1, I-40127 Bologna, Italy

[2]Osservatorio Astronomico di Bologna, via Ranzani 1, I-40127 Bologna, Italy

[3]Osservatorio Astronomico di Collurania, via M. Maggioni, I-64100 Teramo, Italy

[4]European Southern Observatory, Karl-Schwarzchild-Strasse 2, D-85748 Garching bei Munchen, Germany

[1]Based on FLAMES/GIRAFFE observations collected with the Very Large Telescope at the European Southern Observatory, Cerro Paranal, Chile, within the observing programs 71.D-0217(A) and 74.D-0369(A).

($M \sim 2.9\ 10^6 M_\odot$, Merrit et al. 1997), represents one of the most intriguing brain teasers of stellar astrophysics. The observational evidences collected over the last 40 years indicates that ω Cen is the most peculiar object among galactic star clusters in terms of structure, kinematics and stellar content. It is the only known globular cluster which shows a clear metallicity spread. In the last ten years, extensive spectroscopic surveys have been performed on large samples of giant stars (Norris, Freeman & Mighell 1996, Suntzeff & Kraft 1996, hereafter NFM96 and SK96 respectively), showing a multimodal distribution of heavy-element.

Recent photometric surveys have revealed the presence of several anomalous sequences in the color-magnitude diagram (CMD). In particular, wide-field photometric studies (Lee et al. 1999, Pancino et al. 2000 – hereafter P00) have shown the presence of an additional anomalous Red Giant Branch (hereafter RGB-a). According to P00, this population contains approximately 5% of the cluster's stellar content and represents the extreme metal-rich end of the metallicity distribution. Moreover, the metal-rich giants appear to have different spatial distribution and dynamical behaviour with respect to the metal poor ones (Norris et al. 1997, Jurcsik 1998, Pancino et al. 2000, 2003, Sollima et al. 2005a). Beside the dominant population (having metallicity $[Fe/H] \sim -1.6$) and the RGB-a ($[Fe/H] \sim -0.6$), three metal-intermediate (MInts) components (with $-1.3 < [Fe/H] < -1.0$) have been identified by Sollima et al. (2005a, hereafter S05). More recently, a high-precision photometric survey in the central region of the cluster (Ferraro et al. 2004, hereafter F04) revealed the presence of a narrow well defined Sub Giant Branch (SGB-a) which merges into the Main Sequence (MS) of the dominant cluster population at a magnitude significantly fainter than the cluster Turn-off (TO). Although this feature seems to be the extension of the RGB-a, a direct comparison of the MS-TO morphology with theoretical isochrones shows that the anomalous metal-rich population cannot be significantly younger than the most metal-poor one. This interpretation leads to inconsistences with the self-enrichment scenario proposed for ω Cen (Freeman 1993, Lee et al. 1999, Bekki & Freeman 2003). Finally, Anderson (2002) and Bedin et al. (2004) discovered new peculiarities also along the MS of the cluster. In fact, an additional less populous blue Main Sequence (bMS, comprising $\sim$ 30% of the whole cluster MS stars) located parallel to the dominant one, has been evidenced. According to stellar models with canonical chemical abundances, the location of the observed bMS would suggest a lower metallicity. Conversely, Piotto et al. (2005, hereafter P05) presented the spectroscopical analysis of 34 MS stars belonging to the two MS components showing that the bMS stars present a metallicity ~ 0.3 *dex* higher than the dominant cluster population. This evidence brought P05 to conclude that only a large helium enhancement could explain the anomalous position of the bMS in the CMD, as suggested by Norris (2004, hereafter N04) and Lee et al. (2005).

Until now, only rough estimates of the relative ages of ω Cen have been made, using broad and narrow band photometry (Hilker & Richtler 2000, Rey et al. 2004, Hughes et al. 2004). These studies suggested a time scale of chemical enrichment up to 6 Gyr. A smaller age spread ($\sim$ 2 Gyr) has been estimated by N04, Hilker et al. (2004) and Lee et al. (2005), assuming different helium abundances among the stellar populations of ω Cen. In particular, Hilker et al. (2004) estimated an age difference $\Delta t \sim 1.6\ Gyr$ between the MP and MInt populations by measuring iron abundances of $\sim$ 400 SGB-TO stars with low resolution line indexes.

As part of a long term project devoted to the detailed study of the properties of different stellar populations in this cluster (see Ferraro et al. 2003), we present low-resolution spectroscopy of 256 SGB stars of ω Cen. We derived metal content and radial velocities for the different sub-populations of the cluster. Using these estimates we derived their relative ages by the comparison with theoretical isochrones.

In §2 we describe the observations and the data reduction techniques. In §3 we present the metallicity distribution for the whole sample. §4 is devoted to the estimation of the relative ages of the observed populations. In §5 we show the dynamical behaviour of the populations of ω Cen as a function of metallicity. Finally, we summarize and discuss our results in §6.

2. Observations and data reduction

Observations were performed during two runs on May 2003, as a part of the Ital-FLAMES Guaranteed Time Observations (GTO), and on February 2005 at the VLT/UT2 at ESO (Cerro Paranal, Chile) equiped with the multi-fiber spectrograph FLAMES/MEDUSA (Pasquini et al., 2003). We used the low resolution grating LR8, which allows a spectral coverage of 1200 Å(between 8200-9400 Å) with a resolving power of $R \sim 6500$. The spectra were obtained combining three 2085 s long exposures secured in good seeing conditions ($FWHM < 0.8$") , reaching an average signal to noise ratio of $S/N \sim 50$ per pixel. We observed two samples of data: *(i) the WFI sample:* 170 SGB stars belonging to two different branches detected in the CMD of P00 located in an external region of ω Cen ($\sim$ 10' away from the cluster centre), and *(ii) the ACS sample:* 110 SGB stars, selected from the ACS@HST photometry by F04, along four well separated branches. The target stars selected on the CMDs are indicated in Fig. 1.

The one-dimensional spectra were extracted with the GIRAFFE pipeline. 16 fibers were dedicated to sky observations in each exposure. An average sky spectrum was obtained and

subtracted from the object spectra, by taking into account the different fiber transmission. The spectra were then continuum normalized and corrected for telluric absorption bands with IRAF. Spectra of two program stars are shown in Fig. 2 to illustrate the quality of our data. The determination of equivalent widths (EWs) and radial velocities was performed on the basis of infrared Ca II triplet lines strength, following the prescriptions of Rutledge et al. (1997, hereafter R97).

2.1. Radial Velocities

In order to determine radial velocities, we cross correlated the spectra of our sample with a high signal to noise ($S/N > 100$) RGB template spectrum (ROA 371, see Pancino et al. 2002, hereafter P02). All spectra were corrected for heliocentric velocity. The correlation function $C(\lambda)$ between the program spectra $P(\lambda)$ and the template spectrum $T(\lambda)$ was calculated as follows

$$C(\lambda) = \sum_{\lambda=\lambda_{templ}^{inf}}^{\lambda_{templ}^{sup}} P(\lambda)T(\lambda - \Delta\lambda)$$

with $\lambda_{templ}^{inf} = 8350\ \mathring{A}$ and $\lambda_{templ}^{sup} = 8750\ \mathring{A}$ for a large range of $\Delta\lambda$ values (± 10Å). The correlation function $C(\lambda)$ was then fit with a gaussian function whose center provided the velocity estimate. This procedure was performed independently on each single exposure and the root mean square (rms) computed from the mean was assumed as the velocity error. The final Δv_r estimate was used to doppler-shift the spectra at the wavelength corresponding to $v_r = 0$, so that the band windows used to calculate the EWs were properly aligned. All stars with radial velocity different from the mean cluster velocity by more than 2σ were considered field stars. Adopting this criterion, 256 out of a total of 280 stars were retained as bona fide cluster members.

2.2. Ca Index measurement

We measured the EW of three Ca II lines and defined an *equivalent line strength index* ($\Sigma\ Ca$) according to R97:

$$\Sigma\ Ca = 0.5W_{8498} + W_{8542} + 0.6W_{8662}$$

Where W_{8498}, W_{8542} and W_{8662} are the EWs of the CaII lines at $8498\mathring{A}, 8542\mathring{A}$ and $8662\mathring{A}$ respectively. The measurement of the EW of each Ca II line was done by linearly interpolating the average intensities in two continuum bands on each side of the feature. The EW was

the integral over the line band of the difference between the continuum and the line. The band limits used to define the continuum and the feature regions are listed in Table 1. The line profile was modeled with a Moffat function of exponent 2.5 as indicated by R97. For each program star, the three exposures were averaged in order to obtain a higher signal to noise spectrum. The index measurement was performed independently on each single exposure and on the averaged spectrum. We adopted the $\Sigma\ Ca$ index derived from the averaged spectrum as reference, and the rms computed from the three exposures has been assumed as $\Sigma\ Ca$ error.

In all previous Ca II triplet analysis performed on globular cluster RGB stars, the obtained $\Sigma\ Ca$ indices were converted into "reduced" EW using an empirical linear relation linking the $\Sigma\ Ca$ index with the V magnitude difference between the program star and the horizontal branch (HB) of the cluster (Armandroff & Da Costa 1991, Da Costa & Armandroff 1995, Geisler 1995, R97, Cole et al. 2004). This correction removes the gravity effect on EW that, for giant stars, increases approximately linearly with magnitude, with a negligible dependence on temperature (Idiart et al. 1997). Unfortunately, as gravity increases, this approximation holds no more (SK96, Cenarro et al. 2001 – hereafter C01). For this reason we decided to re-calibrate the relation linking $\Sigma\ Ca$ with metallicity, using the most extensive catalog of observed spectra available in the literature by C01. A detailed description of the calibration procedure is provided in Appendix A.

3. Metallicity distribution

Fig. 3 shows the metallicity distribution obtained for the 152 member stars belonging to the *WFI sample*. A sharp and asymmetric peak at [Fe/H] ~ -1.7 can be seen, with a long tail extending toward higher metallicity ([Fe/H] > -1.4), in agreement with the previous spectroscopical determinations by NFM96 and SK96. Care must be taken when comparing the metallicity distribution shown in Fig. 3 with those obtained by NFM96 and SK96, since the present analysis is based on a *biased* sample, formed by targets selected along the different SGBs of ω Cen. Nevertheless, the global shape of the distribution in Fig. 3, is consistent with those showed by NFM96 and SK96.

A more detailed insight on the metal-rich populations of ω Cen can be achieved by observing the average metallicity of stars belonging to the different branches in the *ACS sample* (see Fig. 4). It is worthy of notice that stars selected along different branches in the CMD are confirmed to belong to different metallicity groups. In particular, stars standing on the two brightest SGBs have a mean metallicity of [Fe/H]~ -1.7 and [Fe/H]~ -1.4 respectively, in full agreement with the results obtained using the *WFI sample*. Stars located on the two

faintest SGBs have an average metallicity of [Fe/H] $\sim$ -1.1 and [Fe/H] $\sim$ -0.6, respectively. By comparing the obtained metallicities with the metallicity groups identified on the RGB of ω Cen by S05, we can associate the dominant metal-poor group ([Fe/H] $\sim$ -1.7) to the RGB-MP population and the secondary metal-rich one ([Fe/H] $\sim$ -1.4) to the RGB-MInt2 population. Concerning the group of stars with [Fe/H] $\sim$ -1.1, S05 found a bulk of RGB stars with similar metallicity. A direct comparison with the existing high-resolution spectroscopical analysis on RGB stars in ω Cen confirms the presence of a number of stars with metallicity [Fe/H] $\sim$ -1.0 (Norris & Da Costa 1995, Vanture et al. 2002, P02, Pancino 2003). Given its metal content, we can therefore associate this population of SGB stars to the RGB-MInt3 population, as defined by S05. SGB-a stars, located on the faintest SGB, have a significantly higher metallicity ($\sim$ 1 dex) with respect to the bulk population, representing the extreme metal-rich extension of the stellar content of ω Cen, fully consistent with the measures obtained by P02 for RGB-a stars. *This result represents the first direct confirmation that the RGB-a and the SGB-a sequences belong to the same population.* For clarity, in the following we will adopt for the different populations the naming convention defined by S05. The adopted metallicities for the observed populations of ω Cen are summarized in Table 2.

4. Relative ages

The SGB-TO is the most sensitive region of the CMD to the age of a stellar population. Once the metal content of each SGB population has been measured, we should be able to derive relative ages for each population through an appropriate comparison with theoretical isochrones.

We used a set of theoretical isochrones calculated adopting the most up-to-date input physics (Straniero, Chieffi & Limongi 1997). In particular, the equation of state includes the electrostatic correction (see Prada Moroni & Straniero 2002) and microscopic diffusion (gravitational settling and thermal diffusion). The theoretical isochrones have beed transformed into the observational planes by means of the synthesis code described in Origlia & Leitherer (2000) and using the model atmospheres by Bessel, Castelli & Plez (1998, hereafter BCP98). For the ACS data set, the filter responses and camera throughputs, kindly provided by the ACS User Support Team, have been used.

To compare the observed SGBs with theoretical isochrones, we need to assume a distance modulus and a reddening correction. In the following we adopt the distance modulus by Bellazzini et al. (2004), $(m - M)_0 = 13.70 \pm 0.13$. Concerning the reddening and extinction coefficients, we assumed $E(B - V) = 0.11 \pm 0.01$ (Lub 2002), $A_B = 4.1\ E(B - V)$, $A_R =$

2.35 $E(B-V)$ (Savage & Mathis 1979) and $A_I = 1.8\ E(B-V)$ (Dean, Warren & Cousins 1978).

4.1. Chemical assumptions

Although the evolution of a star along the SGB depends mainly on age and metallicity, other factors may have a non negligible impact, namely the α-elements and helium abundance. Straniero & Chieffi (1991) and Salaris, Chieffi & Straniero (1993) showed that, when computing the isochrones of Population II stars, the contribution of the α-element enhancement can be taken into account by simply rescaling standard models to the global metallicity [M/H], according to the following relation

$$[M/H] = [Fe/H] + log(0.638\ \times\ 10^{[\alpha/Fe]} + 0.362)$$

The corresponding metallicity, in terms of mass fraction Z, is

$$Z = (1-Y)\frac{10^{[M/H]+log[Z/X]_\odot}}{1+10^{[M/H]+log[Z/X]_\odot}}$$

where $[Z/X]_\odot = 0.0176$, according to Allende Prieto et al. (2002) and Asplund et al. (2004). We adopted $[\alpha/Fe] = +0.3$ for both the MP and the MInts population samples, according to the most recent high-resolution spectroscopic results (Norris & Da Costa 1995, Smith et al. 2000, Vanture et al. 2002, P02). For the SGB-a stars, we adopted a significantly lower enhancement $[\alpha/Fe] = +0.1$ as suggested by high-resolution optical spectra (P02) and low-resolution IR spectra (Origlia et al. 2003).

Regarding the helium abundance, several authors considered the effects of differences in helium abundance among the different populations of ω Cen (F04, Bedin et al. 2004, D'Antona & Caloi 2004, N04, P05, Lee et al. 2005). In particular, N04 ad Lee et al. (2005) suggested a helium enhancement of $\Delta Y \sim 0.12$ for the MInt population and $\Delta Y \sim 0.15$ for the most metal-rich anomalous one, in order to reproduce the complex MS morphology of ω Cen. Although such high helium enhancements would imply a series of problems, concerning the helium yields for low-mass stellar systems (see §6), we explored this possibility for the MInts and SGB-a populations by fitting the observed SGBs with models having canonical He abundance and various He-enhancement levels. The adopted metallicity, $[\alpha/Fe]$, Y and the derived age for each population of ω Cen are summarized in Table 2.

4.2. Results

Fig. 5 and 6 show the isochrone fitting for the observed populations of ω Cen for the *WFI sample* and the *ACS sample* respectively, assuming for each population different helium abundances ranging from the cosmological value Y=0.246 (Salaris et al. 2004; Cyburt et al. 2003) up to Y=0.40 . Regarding the *WFI sample*, in order to perform a meaningful comparison and to avoid spurious contamination from stars with uncertain metallicity measurement, we considered only stars with [Fe/H]< -1.8 (SGB-MP population) and $-1.4 <$[Fe/H]< -1.0 (SGB-MInt2 population). As can be seen from Fig. 5, apart from the presence of few outliers (probably due to spectroscopic and/or photometric errors), there is a clear segregation between the two samples. While most of the SGB-MP stars populate the brighter portion of the SGB, SGB-MInt2 stars appear to be mainly located in the fainter part of the SGB. The two groups of stars are fit by theoretical isochrones of the same age (16 Gyr) and appropriate metallicity (see §4.1). In Fig. 5b an isochrone with a significant helium enhancement (Y=0.35) is also overplotted. As can be seen, the location of the target stars is nicely reproduced by this isochrone. The same procedure has been followed for the *ACS sample* (see Fig. 6). Also in this case a set of 16 Gyr old isochrones with appropriate metallicities and different helium enhancements are overplotted. As can be noted, the adoption of a different helium abundance yields a better fit of the SGB shape but does not significantly affect the relative ages. Note that all the populations are nicely reproduced by isochrones with the same age. In order to further support this result, we plotted the four isochrones with the best choice of helium abundance, as derived from the comparison shown in Fig. 5b and 6, and various ages in Fig. 7. As can be seen, a change of $\pm 2 Gyr$ in the adopted age produces a significant variation in the isochrone location. Hence, the average error in the age differences, estimated on the basis of the effects produced on the estimated age by the intrinsic magnitude spread of the observed SGBs, can be assumed to be $\sim 1.5\ Gyr$. Summarizing, we reproduced all the four considered populations with 16 Gyr old isochrones. The adopted He abundances are: the cosmological Y=0.246 for the SGB-MP population, Y=0.35 for the SGB-MInt2 population, Y=0.35 for the SGB-MInt3 population and Y=0.40 for the SGB-a population. We found that a large helium enhancement affects the morphology of the SGB but does not change its average magnitude. In particular, increasing the helium abundance:

- The slope of the SGB becomes steeper;
- The color difference between the TO and the RGB base decreases.

As a consequence, the assumption of a differential helium abundance among the different populations of ω Cen allows a better fit of the observed SGB morphology but does not

significantly affect the relative ages.

Note that although the old zero point of the adopted age scale differs from the most recent determinations of the age of the universe (Cyburt et al. 2003), the age differences are marginally affected by this assumption.

In Fig. 8 the four isochrones are overplotted to the entire ACS CMD of ω Cen. The isochrones correctly reproduce the global shape of the observed sequences from the MS up to the RGB. However, is worth of noticing that:

(i) Our best-fit isochrone for the MInt2 population, having Y=0.35, does not cross the MP isochrone at the MS level. If we accept the hypotesis that the MInt2 population is related to the blue MS observed by Bedin et al. (2004), we need to adopt a larger helium abundance ($Y_{MInt2} > 0.35$) in agreement with what found by N04, P05 and Lee et al. (2005).

(ii) Together with isochrones, the Zero Age Horizontal Branch (ZAHB) of the MP and MInt2 populations are plotted on the CMD. We used the latest models computed using FRANEC (see Straniero, Chieffi & Limongi 1997 for details) [2]. As can be immediately noted, the ZAHB corresponding to the MInt2 population is significantly brighter than the observed HB. This is a consequence of the large helium abundance assumed for this population, that strongly increases the CNO cycle efficiency in the HB stars envelopes and leads to a stable equilibrium stage at higher luminosity. Butler et al. (1978) and Rey et al. (2000) found a group of RR Lyrae variables with metallicity significantly higher than that of the dominant cluster population located ~ 0.3 *mag* below the average RR Lyrae V magnitude. If we associate the metal-rich RR Lyrae to the MInt2 population, the assumption of a significant increase in the He abundance would produce a stark incongruence with the observed luminosity of such metal-rich RR Lyrae. Similar incongruences between the expected and the observed luminosity of metal-rich RR Lyrae stars have been noted by N04 and Sollima et al. (2005b in preparation). In this respect, note that most of the helium-rich HB stars reach higher temperatures because of their smaller masses, and therefore populate essentially the blue tail of the HB, a region where magnitude differences cannot be appreciated (P05, Lee et al. 2005). Hence, only few helium-rich stars are expected to cross the instability strip.

[2]The ZAHB were calculated by interpolating the location in the CMD of the tracks of stars with masses ranging from 0.52 to 0.80 $M_{\odot}$. The core masses and the surface compositions were derived from the corresponding last models in the H-burning shell. The ZAHB model was set when all the secondary elements in their H-burning shell are relaxed to their equilibrium values.

5. Kinematics

Another intriguing characteristic of ω Cen is the observed connection between kinematics and abundances. From Ca II triplet analysis of about 400 RGB stars, Norris et al. (1997, hereafter N97) found that the 20% metal-rich tail of the metallicity distribution is kinematically cooler than the 80% metal poor component. Beside this result, N97 found that their metal-rich component does not show the same systemic rotation as the metal-poor one. This last finding appears in contradiction to a simple dissipative scenario. We used our sample to find further evidences of such behaviour. Fig. 9 shows the radial velocity and velocity dispersion as a function of metallicity for the global sample of stars presented in this paper. The mean radial velocity of the whole sample is $v_r = -235.9 \pm 0.8\ Km\ s^{-1}$ and the average dispersion $\sigma_{v_r} = 12.6\ Km\ s^{-1}$. SGB-a stars present no significant radial velocity offset with respect to the bulk population stars, having $v_r^{SGB-a} = -236.5 \pm 1.7\ Km\ s^{-1}$.

A surprising result concerns the behaviour of the velocity dispersion as a function of metallicity. As can be seen from Fig. 9b, for stars with $-1.7 < [Fe/H] < -1.0$, the velocity dispersion decreases as the metal abundance increases, in agreement with the result by N97. SGB-a stars do not follow this trend: they show a significantly larger velocity dispersion and seem to be kinematically warmer than the MInt stars. This evidence is confirmed even if we consider only stars lying in the inner $5'$, and seems to be independent on the distance to the cluster center. Although the sample used by N97 spans a metallicity range similar to that covered by the present analysis (-1.6 $< [Ca/H] <$ 0.0), it contains only a few stars at [Ca/H] > -0.7. For this reason, while at metallicity $-2.0 < [Fe/H] < -1.0$ the trend observed by N97 is fully confirmed by our analysis, the peculiar kinematical behaviour of SGB-a stars could not be detected by N97. Summarizing, the MInt populations are the only cool components, being kinematically cooler than both the (hot) MP population and the (warm) SGB-a. The observed behaviour of the kinematical properties of ω Cen as a function of its metallicity is still far from being fully understood.

The warm velocity dispersion of the SGB-a stars adds up to other structural and kinematical peculiarities of the RGB-a stars. First, the RGB-a centroid in the spatial density distribution appears significantly dislocated from the main population's one (Pancino et al. 2003, S05). Moreover, the mean proper motion of RGB-a stars differs significantly from that of the main cluster population (Ferraro et al. 2002). This last result has been questioned by Platais et al. (2003) who claimed that the different proper motion observed for RGB-a stars is due to a spurious instrumental effect in the original proper motion catalog by van Leuween et al. (2000). However, while the arguments of Platais et al. (2003) were already considered and dismissed in the original publication by van Leuween et al. (2000), they also have been strongly criticized by Hughes et al. (2004), who quantitatively demonstrated that

the original proper motion catalogue is free from any spurious instrumental trend. Further support to the correctness of the proper motion measurements has been brought by Pancino (2003), who again did not found any significant proper motion variation with neither magnitude nor color.

6. Discussion and Conclusions

We presented low-resolution spectroscopy of 256 SGB stars in ω Cen. Metallicities and radial velocities have been measured from Ca II triplet lines analysis. The metallicity distribution function confirms the metallicity spread observed in previous analysis performed on giant stars. SGB-a stars appear to have a metallicity higher than the bulk population, representing the extreme metal-rich extension of the stellar content of ω Cen. The relative ages of the different stellar populations of the system have been estimated by fitting the observed SGBs with theoretical isochrones having appropriate metallicities and various helium content. The ages derived for the different populations are all compatible within 2 Gyr. This result indicates that ω Cen enriched itself in a short timescale ($< 2\ Gyr$) and imposes firm constraints on the chemical evolution of the system.

The hypotesis of a large helium gradient between the populations of ω Cen has been tested. We found that the morphology of the SGB of the most metal rich populations of the cluster can be better reproduced assuming a helium enhancement, with respect to the dominant metal poor population, of $\Delta Y \sim 0.10 - 0.15$ for the MInts population and $\Delta Y \sim 0.15 - 0.20$ for the anomalous one, in good agreement with previous estimates in literature. Such large helium overabundances do not affect significantly the relative ages of the stellar populations.

The results presented here exclude an extended star formation period, regardless of the adopted helium abundances. The average error in the age differences is $\sigma_{\Delta t} \sim 1.5\ Gyr$ (see §4.2), so age differences smaller than this quantity cannot be appreciated. Nevertheless, this finding imposes serious problems related to the chemical enrichment history of this stellar system. Hilker & Richtler (2000) claimed an extended star formation period in order to explain the tight correlation between CN-band strengths and iron abundances. Moreover, the abundance patterns of s-process elements require the contribution of low-mass AGB stars ($1.5 \div 3 M_{\odot}$, Smith et al. 2000). Stars of these masses reach the AGB phase after 0.7 - 1.5 Gyr that should represent a lower limit for the age difference between the populations of ω Cen. Finally, in the hypotesis of a large helium enhancement, the derived helium abundance gradient between the MP and MInt2 population turns out to be $\delta Y/\delta Z \sim 180$, in stark contrast with more canonical values of $\delta Y/\delta Z \sim 3 - 4$ (Pagel et al. 1992, Jimenez et al.

2003). An efficient He production driven by low-mass AGB stars would be accomplished by a corresponding C overabundance, in contradiction with observational evidences (Smith et al. 2000). In the same way, intermediate mass stars would produce, beside He, an unusual N abundance. A larger helium yield is provided by more massive objects (M > $20M_{\odot}$) wherein black hole production limits the amount of heavy elements relative to helium in the ejecta released into the interstellar medium (Timmes et al. 1995).

The kinematics of the stellar populations of the cluster appear more puzzling than ever. The velocity dispersion as a function of metallicity shows a mimum at $[Fe/H] \sim -1.1$, suggesting that MInt populations are kinematically cooler than both the MP and the anomalous population.

The emerging scenario can be summarized as follows:

i) The MP population ([Fe/H] $\sim$ -1.7) represents the first and largest event of star formation of ω Cen. It contains the majority of cluster's stars, and can be well reproduced by an old isochrone having a cosmological helium abundance. Moreover, it presents the highest velocity dispersion among the different cluster populations.

ii) The MInt2 population ([Fe/H] $\sim$ -1.3) could have had a peculiar history. It is suspected to be connected to the bMS (Bedin et al. 2004, P05), and for this reason it requires an anomalous helium overabundance (Y > 0.35). This population formed after a short timescale (< 2 Gyr) from a medium enriched by SNII in iron and α-elements abundance, and by AGB winds of massive stars in s-process elements and, possibly, helium (see also the discussion in §4.2). How a such huge amount of helium could have been produced remains at present an unanswered question. Moreover, MInt2 stars present a smaller velocity dispersion with respect to the bulk metal poor population ones, indicating an evolution in the dynamical settling of the system. The MInt3 population ([Fe/H] $\sim$ -1.0), together with MInt2, represents the kinematically cool component.

iii) The anomalous population represents the metal-rich end of the stellar population mix of ω Cen at [Fe/H] $\sim$ -0.6. Although increasing the Helium abundance to Y$\sim$0.4 improves the fit of the SGB-a shape, no value of Helium abundance can make this anomalous population significantly younger than the MP population. Moreover, the analysis of radial velocities of these stars indicates a kinematical behaviour different from the MInt populations. For these reasons, the understanding of the origin and evolution of this population is still a mistery.

Two different scenarios can be put forward to explain its origin:

a) A very fast self-enrichment process generated the anomalous population in the early stage of evolution of ω Cen, producing a large amount of helium ($\Delta Y \simeq 0.4$), s-process

elements ([s/Fe] $\simeq$ +1.0) and iron (leading to a lower [α/Fe]$\simeq$ +0.1) in less than 2 Gyr.

b) The anomalous population evolved in a different environment and was later accreted by the main body of ω Cen.

Freyhammer et al. (2005) suggested that stars belonging to the SGB-a are physically separated from and more distant than the main body of ω Cen by about 120-250 pc. To achieve their best fit under this hypothesis, however, the authors have to assume for the SGB-a a metallicity of –1.1<[Fe/H]<–0.8, in stark contrast with the present determination, and the abundance measured along the RGB-a ([Fe/H]$\simeq$–0.6$\pm$0.15, P02 and Origlia et al. 2003). Moreover, the few radial velocity determinations of RGB-a stars (P02, Vanture et al. 2002 and Origlia et al. 2003) and the present large sample of SGB-a measurements suggest that the radial velocity of this population is not different from the ω Cen systemic velocity, therefore implying that SGB-a stars and ω Cen are at least dynamically bound to each other.

The results presented in this paper confirm once more that a simple self-enrichment scenario cannot explain all the observational evidences gathered in the past. Many questions remain to be understood in order to explain the formation and evolution of this peculiar stellar system. Therefore, it is clear that if one desires to accommodate all the observational facts in one self-consistent scenario, it is necessary to include not only a complex chemical evolution, but also a complex dynamical history.

This research was supported by the Ministero dell'Istruzione, dell'Università e della Ricerca. We warmly thank Paolo Montegriffo for assistance during the catalogs cross-correlation and astrometric calibration process and Luciano Piersanti for his helpful support in the theoretical tracks calculations. We thank also the anonymous referee for his helpful comments and suggestions. AS acknowledge the *Marco Polo Project* for the financial support and the European Southern Observatory in Garching for the hospitality during his stay.

A. Calibration of the $\Sigma\ Ca$-[Fe/H] relation

In this appendix we present the $\Sigma\ Ca$ index calibration as a function of metallicity for sub-giant stars, as derived from the application of the *running box technique* to the most extensive catalog of spectra available in literature (C01).

Since the EW measurement technique and index definition by C01 are slightly different from the *equivalent line strength index* $\Sigma\ Ca$ defined in §2.2, as first step we measured $\Sigma\ Ca$ as defined in §2.2 on the 603 spectra of C01. Fig. 10 shows the location of the C01 stars in the $\Sigma\ Ca$ – [Fe/H] plane, where different symbols are used for stars in different gravity

ranges. As expected, in the metallicity range –2.8<[Fe/H]<-0.4, the $\Sigma\ Ca$ index increases approximately linearly with metallicity. For stars with higher metallicity ([Fe/H] > -0.3) the $\Sigma\ Ca$ index depends mostly on gravity. For very metal-poor stars ([Fe/H] < -3) the Ca II triplet lines strength become insignificant, making it difficult to measure in noisy spectra. In this metallicity range $\Sigma\ Ca$ is expected to correlate with metallicity in an asymptotic way.

The $\Sigma\ Ca$ index measured in the ω Cen targets cover the range 0.8Å< $\Sigma\ Ca$ <3.7Å. In this range the dependence of metallicity on $\Sigma\ Ca$ can be reasonably approximated by a linear relation. However, the effect of gravity is non-negligible and can significantly affect such a relation. For this reason, we decided to further investigate the parameters space occupied by our target stars in the $(T_{eff}, \log\ g)$ plane.

Temperatures were derived using the color-temperature conversion provided by BCP98. Gravities were derived from the universal gravitation law assuming a mass of 0.8 $M_{\odot}$ (Bergbusch & VandenBerg 2001) and the temperatures derived above. We used the BVI magnitudes by P00 for the *WFI sample*, while for the *ACS sample* stars we used the BR magnitudes by F04 in order to derive temperatures and gravities, once the BCP98 conversions have been corrected for the ACS filter response and camera troughputs (see §4). Fig. 11 shows the location of the target stars of ω Cen (*open circles*) with respect to the C01 stars (*filled circles*) [3]. As can be seen, the bulk of the target stars covers the range $3 < \log\ g < 4$ and $4600\ K < T_{eff} < 6000\ K$. Only a bunch of C01 stars are present in this range. For this reason we decided to apply the so-called *running box technique* to the $(T_{eff}, \log\ g)$ plane in order to derive appropriate $\Sigma\ Ca$ – [Fe/H] relations. A sampling box with $\Delta T_{eff} = 1700\ K$ and $\Delta \log\ g = 1.2\ dex$ has been defined and moved in steps of $\delta T_{eff} = 400\ K$ and $\delta log\ g = 0.3\ dex$, scanning the entire area covered by the C01 sample in the $(T_{eff}, \log\ g)$-plane (Fig. A2). All the C01 stars (with EW in the range 0.8 Å< $\Sigma\ Ca$ <3.7 Å) lying in each box have been used to derive a linear regression relation between $\Sigma\ Ca$ and [Fe/H]. Finally, a general fitting function for the whole parameter space has been constructed by smoothing the derived local functions with a gaussian filter. For a given point in the parameter space with coordinates $P(\log\ g, T_{eff}, \Sigma\ Ca)$ we computed the corresponding value of metallicity $[Fe/H]_i$, for each box containing it. A gaussian-weighted average of the various $[Fe/H]_i$ corresponding to all the boxes containing P yields the final metallicity, defined as follows:

[3]Before applying the calibration, all spectra were smoothed to the resolution of the calibration spectra of C01 ($FWHM \sim 1.5$ Å) and the analysis was repeated in order to measure the shift in the EW measurement due to the different resolution. We find a small $\Sigma\ Ca$ shift of $\Delta\Sigma\ Ca = 0.044 \pm 0.062$ Å, that was applyied to all the $\Sigma\ Ca$ measurements and its error was propagated into the final $\Sigma\ Ca$ error.

$$[Fe/H] = \frac{\sum_i w_i \; [Fe/H]_i}{\sum w_i}$$

where the weight w_i is modulated by the distance of the considered P from the center of the i-th box in the $(log\ g, T_{eff})$-plane

$$w = e^{-(\frac{log\ \ g - log\ \ g_i}{\sigma_g})^2 - (\frac{T - T_i}{\sigma_T})^2}$$
$$\sigma_g = 1.2\ dex$$
$$\sigma_T = 1700\ K$$

In order to check the reliability of the present calibration, we derived the metallicity of all the C01 sample stars using the procedure described above. Fig. 12 shows the difference of metallicity between our determination and the original determination by C01, as a function of the involved parameters ($[Fe/H]$, log g, T_{eff} and $\Sigma\ Ca$, respectively). As can be seen, no significant residual trends are present. The mean dispersion of the fit is 0.15 dex, that can be assumed as the overall accuracy of the calibration.

A.1. Metallicity errors

Several sources of uncertainty occur in the present metallicity determination. In particular:

- Uncertainties in the EW measurements;
- Uncertainties in the resolution correction;
- Photometric errors on the BVRI magnitudes;
- Uncertainties in the color-temperature and magnitude-gravity conversion;
- Uncertainties in the $\Sigma\ Ca$-[Fe/H] calibration.

In order to estimate the overall uncertainty in the derived metallicities, we performed a Monte Carlo simulation spanning a range of $\pm 5\sigma$ in each error source listed above. We assumed the uncertainties on the $\Sigma\ Ca$ as described in the §2.2, the photometric errors given by P00 and F04, the temperature uncertainty reported by BCP98 and propagated into the gravity determination, and the error in the $\Sigma\ Ca$-[Fe/H] calibration as derived in the previous section. The resulting mean error is $\sigma_{[Fe/H]} = 0.2\ dex$.

REFERENCES

Allende Prieto, C., Asplund, M., Garcia Lopez, R. J., & Lambert, D. L., 2002, ApJ, 567, 544

Anderson J. in "ω Centauri: A Unique Window into Astrophysics", 2002, ed. F. van Leeuwen, J. D. Huges & G. Piotto, ASP Conf.Series, 87

Asplund, M., Grevesse, N., Sauval, A. J., Allende Prieto, C., Kiselman, D., 2004, A&A, 417, 751

Armandroff, T. E. & Da Costa, G. S., 1991, AJ, 101, 1329

Bedin, L. R., Piotto, G., Anderson, J., Cassisi, S., King, I. R., Momany, Y. & Carraro, G., 2004, ApJ, 605, L125

Bekki, K. & Freeman, K. C., 2003, MNRAS, 346, L11

Bellazzini, M., Ferraro, F. R., Sollima, A., Pancino, E., Origlia, L., 2004, A&A, 424, 199

Bergbusch, P. A. & VandenBerg, D. A., 2001, ApJ, 556, 322

Bessel, M S., Castelli, F. & Plez, B., 1998, A&A, 333, 231 (BCP98)

Butler, D., Dickens, R. J., Epps, E., 1978, ApJ, 225, 148

Cenarro, A. J., Cardiel, N., Gorgas, J., Peletier, R. F., Vazdekis, A. & Prada, F., 2001, MNRAS, 326, 959 (C01)

Cenarro, A. J., Gorgas, J., Cardiel, N., Pedraz, S., Peletier, R. F. & Vazdekis, A., 2001, MNRAS, 326, 981

Cenarro, A. J., Gorgas, J., Cardiel, N., Vazdekis, A.& Peletier, R. F., 2002, MNRAS, 329, 863

Cole, A. A., Smecker-Hane, T. A., Tolstoy, E., Bosler, T. L., Gallagher, J. S., 2004, AJ, 120, 1808

Cyburt, R. H., Fields, B. D., Olive, K. A., 2003, Phys. Lett. B, 567, 227

D'Antona, F., Caloi, V., 2004, ApJ, 611, 871

Da Costa, G. S. & Armandroff, T. E., 1995, AJ, 109, 2533

Dean, J. F., Warren, P. R. & Cousins, A. W. J., 1978, MNRAS, 183, 569

Ferraro, F. R., Bellazzini, M., Origlia, L. & Pancino, E. in "New Horizons in Globular Cluster Astronomy", 2003, ed. G. Piotto, G. Meylan, S. G. Djorgovski & M. Riello, ASP Conf. Ser., 296, 215

Ferraro, F. R., Sollima, A., Pancino, E., Bellazzini, M., Origlia, L., Straniero, O., Cool, A., 2004, ApJ, 603, L81 (F04)

Freeman, K. C., in "The Globular Cluster-Galaxy Connection", 1993, ed. G. H. Smith & J. P. Brodie, ASP Conf. Ser., 608

Freyhammer, L. M., Monelli, M., Bono, G., Cunti, P., Ferraro, I., Calamida, A., Degl'Innocenti, S., Prada Moroni, P. G., Del Principe, M., Piersimoni, A., Iannicola, G., Stetson, P. B., Andersen, M. I., Buonanno, R., Corsi, C. E., Dall'Ora, M., Petersen, J. O., Pulone, L., Sterken, C., Storm, J., 2005, ApJ, 623, 860

Geisler, D., Piatti, A. E., Clariá, J. J., Minniti, D., 1995, AJ, 109, 605

Hilker, M. & Richtler, T., 2000, A&A, 362, 895

Hilker, M., Kayser, A., Richtler, T. & Willemsen, P., 2004, A&A, 422, L9

Hughes J., Wallerstein G., van Leeuwen F., Hilker M., 2004, AJ, 127, 980

Idiart, T. P., Thévenin, F., de Freitas Pacheco, J. A., 1997, AJ, 113, 1066

Jimenez, R., Flynn, C., McDonald, J. & Gibson, B. K., 2003, Science, 299, 1552

Jurcsik, J., 1998, ApJ, 506, 113

Lee, Y. W., Joo, J. M., Sohn, Y. J., Rey, S. C., Lee, H. C. & Walker, A. R., 1999, Nature, 402, 55

Lee, Y. W., Joo, S. J., Han, S. I., Chung, C., Ree, C. H., Sohn, Y. J., Kim, Y. C., Yoon, S. J., Yi, S. K. & Demarque, P., 2005, ApJ, 621, L57

Merritt, D., Meylan, G. & Mayor, M., 1997, AJ, 114, 1074

Norris, J. E., 2004, ApJ, 612, L25 (N04)

Norris, J. E., Freeman, K. C. & Mighell, K. J., 1996, ApJ, 462, 241 (NFM96)

Norris, J. E., Freeman, K. C., Mayor, M.& Seitzer, P., 1997, ApJ, 487, L187 (N97)

Norris, J. E., Da Costa, G. S., 1995, ApJ, 447, 680

Origlia, L., Ferraro, F. R., Bellazzini, M., Pancino, E., 2003, ApJ, 591, 916

Origlia, L., Leitherer, C., 2000, AJ, 119, 2018

Pagel, B. E., Simonson, E. A., Terlevich, R. J. & Edmunds, M. G., 1992, MNRAS, 255, 325

Pancino, E., Ferraro, F. R., Bellazzini, M., Piotto, G. & Zoccali, M., 2000, ApJ, 534, L83 (P00)

Pancino, E., Pasquini, L., Hill, V., Ferraro, F. R. & Bellazzini, M., 2002, ApJ, 568, L101 (P02)

Pancino, E., 2003, PhD Thesis, Bologna University

Pancino, E., Seleznev, A., Ferraro, F. R., Bellazzini, M. & Piotto, G., 2003, MNRAS, 345, 683

Pasquini, L., Alonso, J., Avila, G., Barriga, P., Biereichel, P., Buzzoni, B., Cavadore, C., Cumani, C., Dekker, H., Delabre, B., Kaufer, A., Kotzlowski, H., Hill, V., Lizon, J. L., Nees, W., Santin, P., Schmutzer, R., Kesteren, A. V., Zoccali, M., 2003, SPIE, 4841, 1682

Piotto, G., Villanova, A., Bedin, L. R., Gratton, R., Cassisi, S., Momany, Y., Recio-Blanco, A., Lucatello, S., Anderson, J., King, I. R., Pietrinferni, A. & Carraro, G., 2004, ApJ, 621, 777 (P05)

Platais, I., Wyse, R. F. G., Hebb, L., Lee, Y. W. & Rey, S. C., 2003, ApJ, 591, L127

Prada Moroni, P., Straniero, O., 2002, ApJ, 581, 585

Rey, S. C., Lee, Y. W., Joo, J. M., Walker, A. R., Baird, S., 2000, AJ, 119, 1824

Rey, S. C., Lee, Y. W., Ree, C. H., Joo, J. M., Sohn, Y. J. & Walker, A. R., 2004, AJ, 127, 958

Rutledge, G. A., Hesser, J. E., Stetson, P. B., Mateo, M. Simard, L., Bolte, M., Friel, E. D., Copin, Y., 1997, PASP, 109, 883 (R97)

Rutledge, G. A., Hesser, J. E., Stetson, P. B., 1997, PASP, 109, 907

Salaris, M., Chieffi, A., Straniero, O., 1993, Mem. Soc. Astron. Italiana, 63, 315

Salaris, M., Riello, M., Cassisi, S. & Piotto, G., 2004, A&A, 490, 911

Savage, B.D., Mathis, J. S., 1979, ARA&A, 17, 73

Smith, V. V., Suntzeff, N. B., Cunha, K., Gallino R., Busso, M., Lambert, D. L. & Straniero, O., 2000, AJ, 119, 1239

Sollima, A., Ferraro, F. R., Pancino E. & Bellazzini, M., 2005a, MNRAS, 357, 265 (S05)

Straniero, O., Chieffi, A., 1991, ApJS, 76, 911

Straniero, O., Chieffi, A. & Limongi, M., 1997, ApJ, 490, 425

Suntzeff, N. B. & Kraft, R. P., 1996, AJ, 111, 1913 (SK96)

Timmes, F. X., Woosley, S. E. & Weaver, T. A., 1995, ApJS, 98, 617

van Leeuwen, F., Le Poole, R. S., Reijns, R. A., Freeman, K. C., & de Zeeuw, P. T., 2000, A&A, 360, 472

Vanture, A. D., Wallerstein, G. & Suntzeff, N. B., 2002, ApJ, 569, 984

This preprint was prepared with the AAS LaTeX macros v5.2.

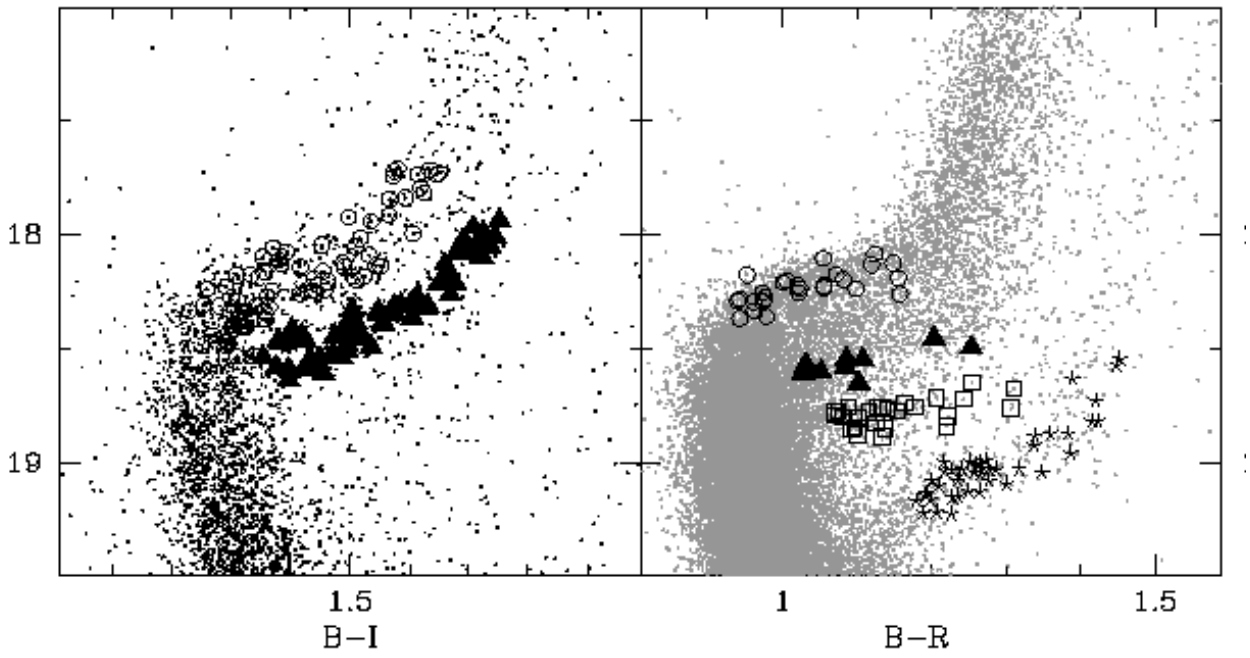

Fig. 1.— The positions of the selected targets are marked in the CMDs of ω Centauri. Stars selected from WFI photometry by P00 are shown in the left *panel*, stars from ACS/HST observations (F04) are marked in the right *panel*. Different symbols indicate the stars selection along different branches: SGB-MP (open circles), SGB-MInt2 (filled triangles), SGB-MInt3 (open squares) and SGB-a (asterisks).

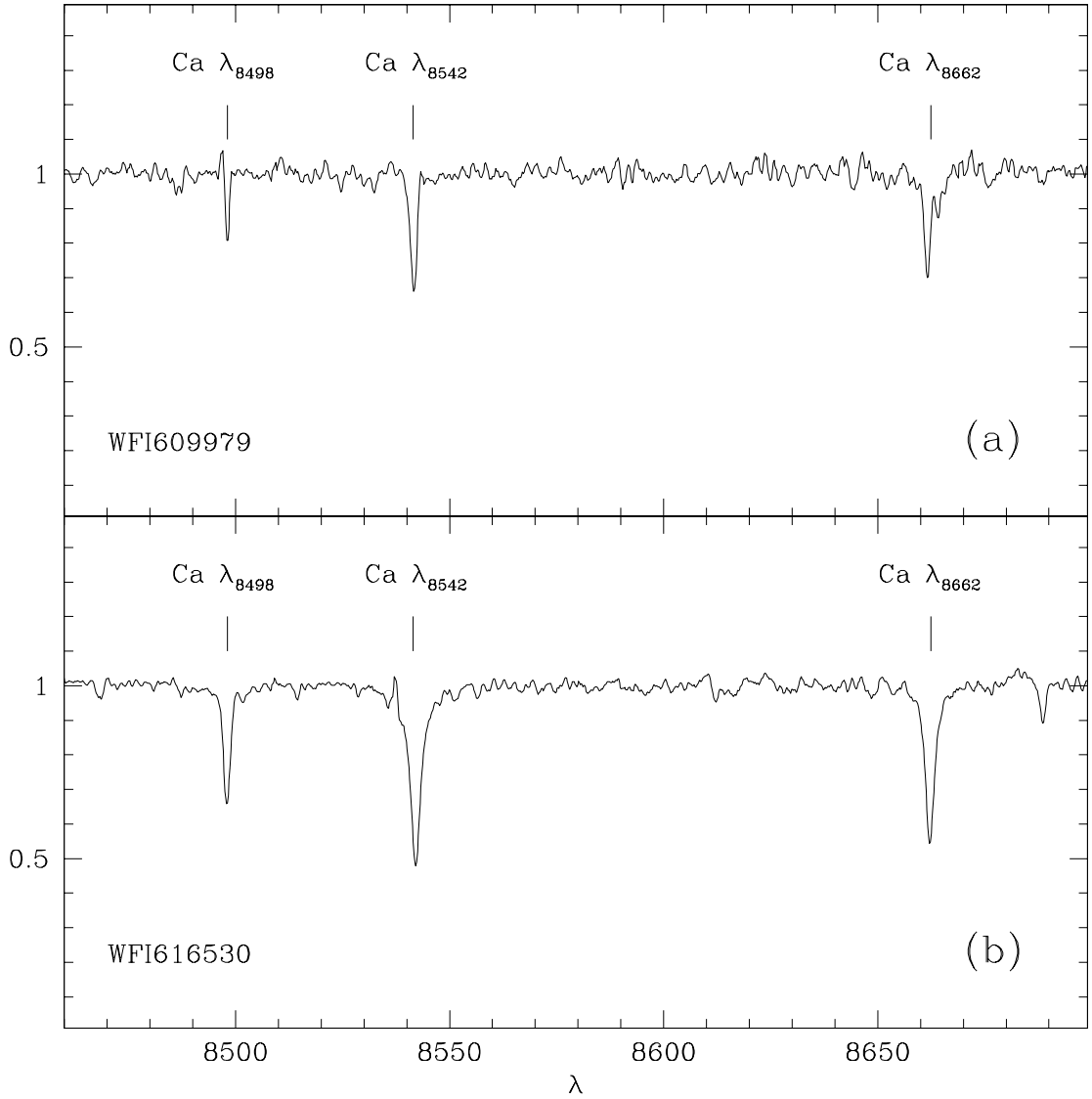

Fig. 2.— Spectra of star WFI609979 ([Fe/H]=-2.15, *panel* a) and WFI616530 ([Fe/H]=-0.97, *panel* b). Ca II triplet lines are indicated.

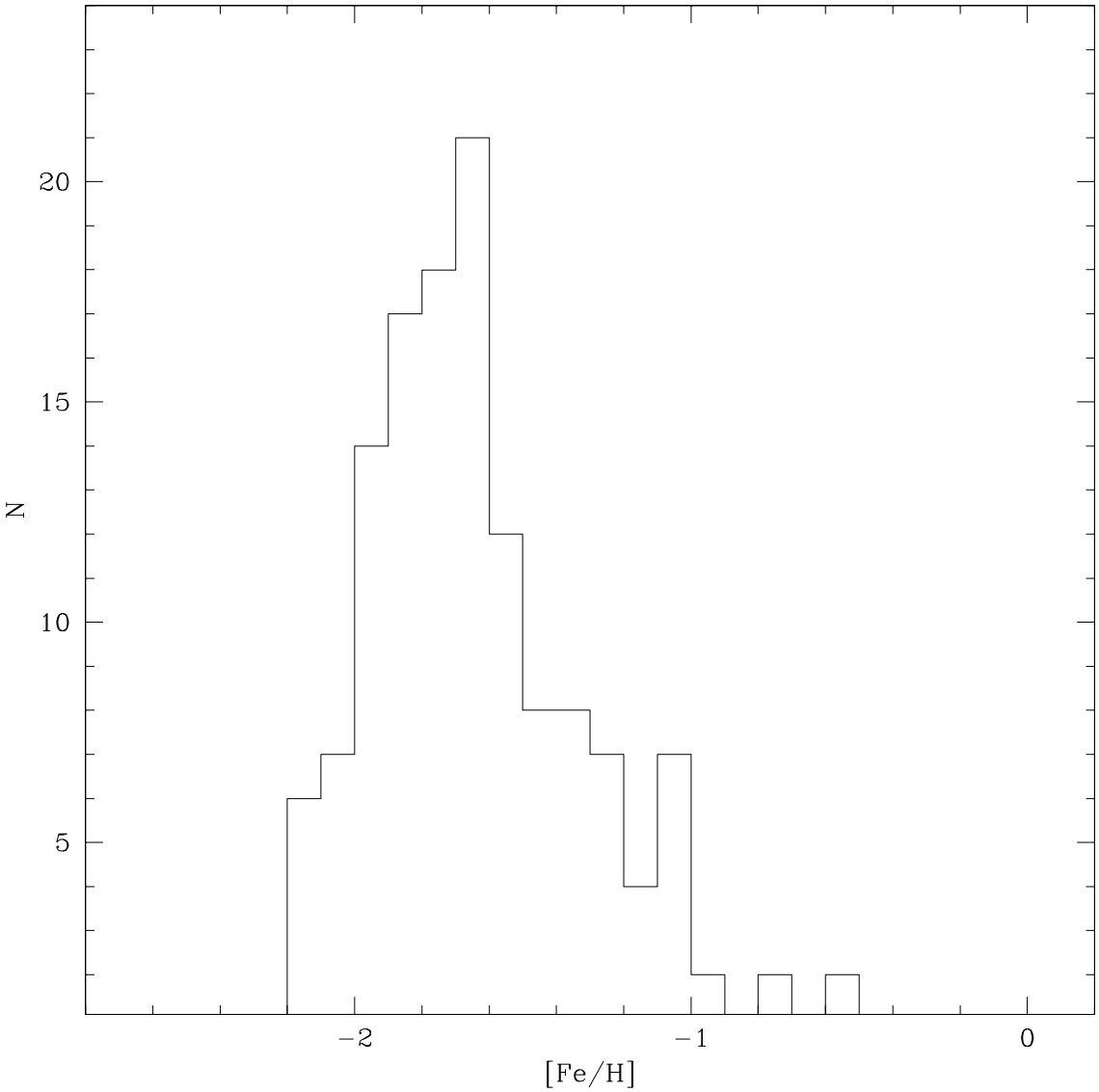

Fig. 3.— The derived metallicity distribution for the 152 cluster member stars in the *WFI sample*.

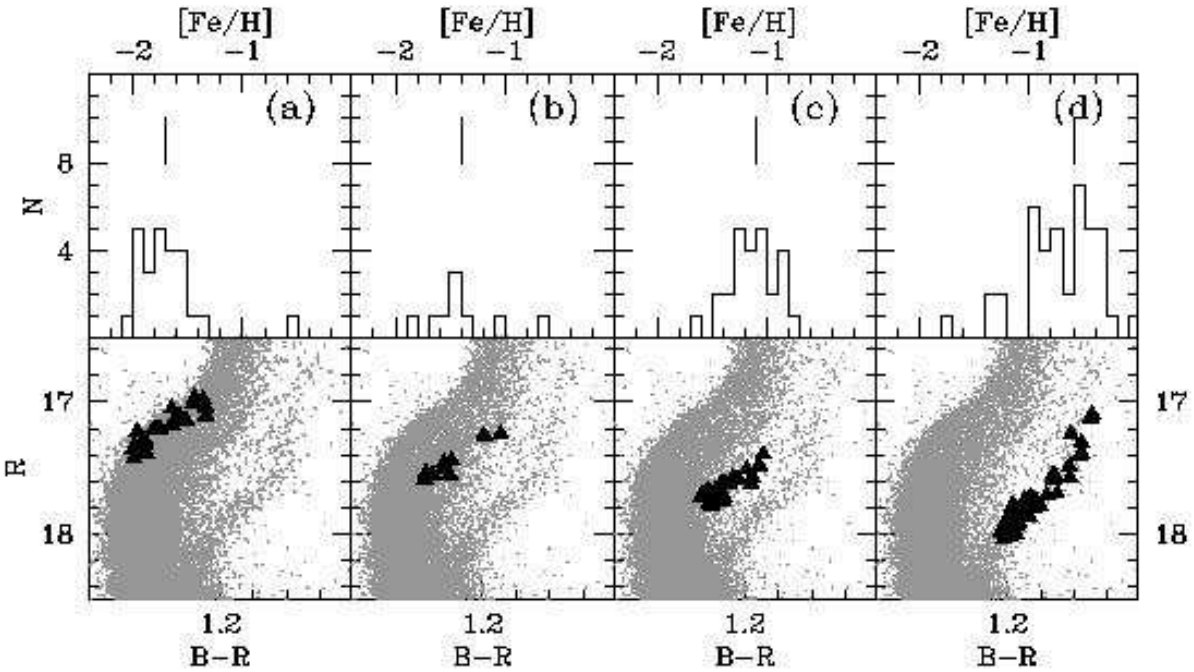

Fig. 4.— Metallicity distributions for the four group of stars selected in the *ACS sample* (upper *panels*). The peak metallicity of each group is indicated. The positions of the selected stars are marked on the ACS CMD (F04) in the corresponding bottom *panels*.

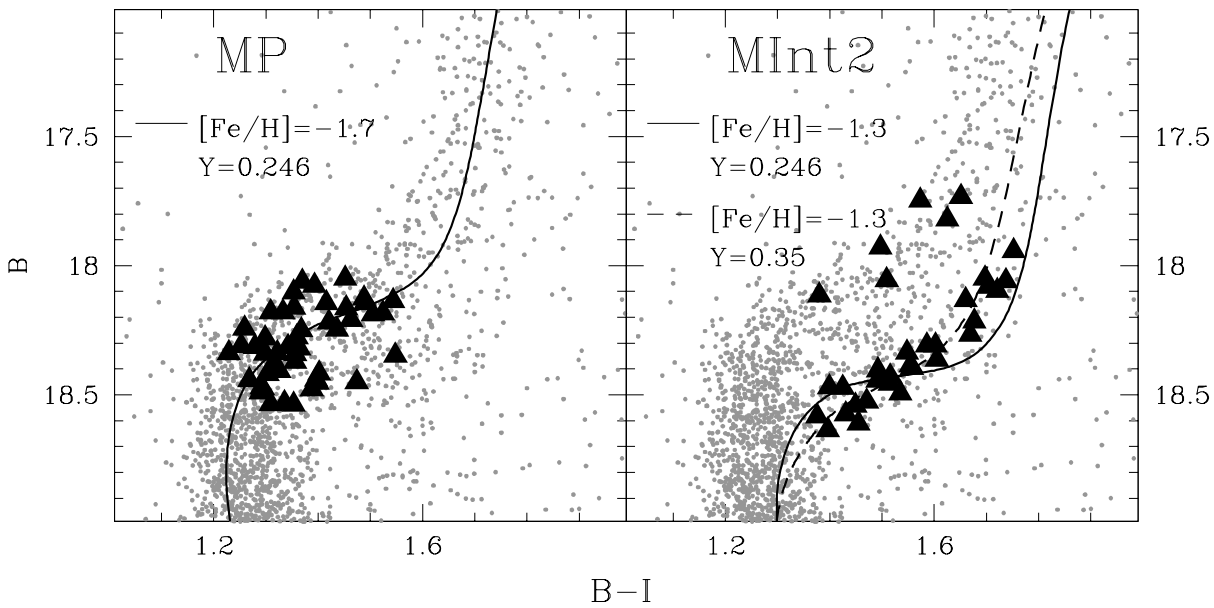

Fig. 5.— Isochrone fitting of the SGB sub-populations in the WFI *sample*. Stars with metallicity $[Fe/H] < -1.8$ ($SGB - MP$) and $-1.4 < [Fe/H] < -1.0$ ($SGB - MInt2$) are plotted as triangles in the *left* and *right panel*, respectively. Theoretical 16 Gyr old isochrones with appropriate metallicity and helium abundance (Y=0.246: *solid lines* and Y=0.35: *dashed line*) are overplotted.

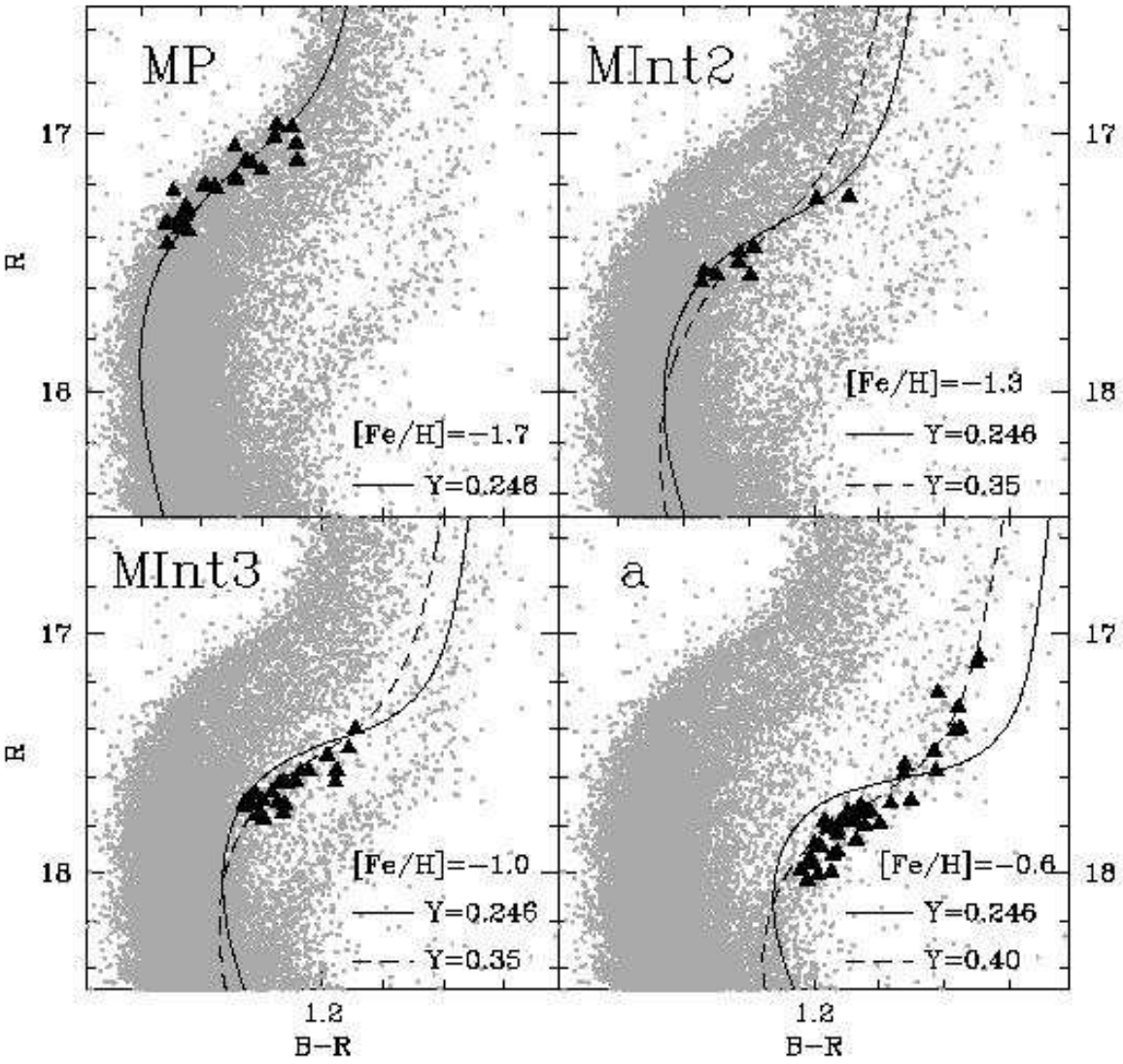

Fig. 6.— Isochrone fitting of the four observed SGBs of ω Cen in the *ACS sample*. The spectroscopic target stars belonging to different sub-populations are marked on the CMD as triangles. Theoretical 16 Gyr old isochrones with appropriate metallicity and helium abundance (Y=0.246:solid lines and different enhanced helium abundances: dashed lines) are overplotted.

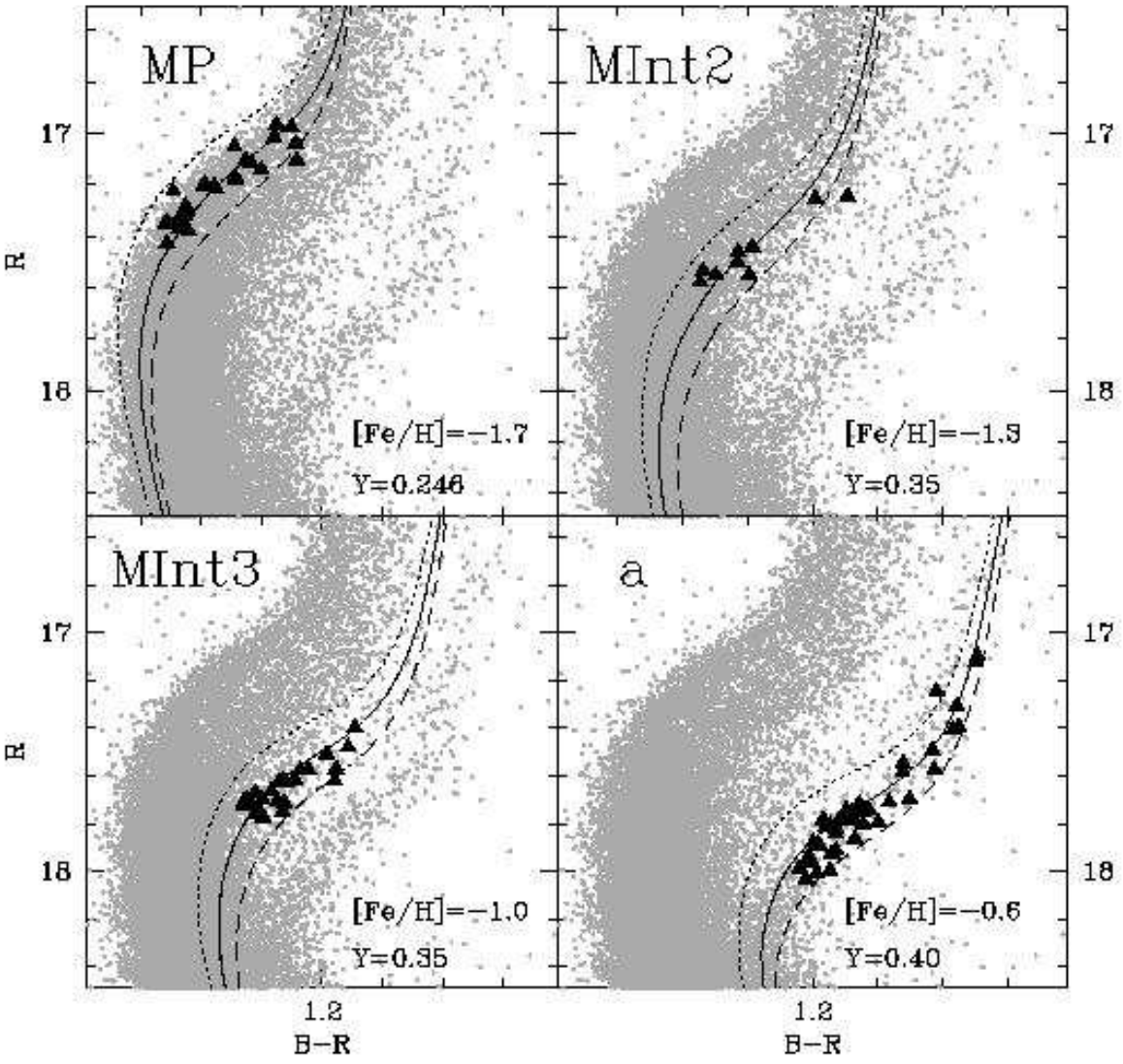

Fig. 7.— Same as Figure 6. Theoretical isochrones with appropriate metallicity and helium abundance (see Table 2) and various ages (14 Gyr dotted lines; 16 Gyr solid lines; 18 Gyr dashed lines) are overplotted.

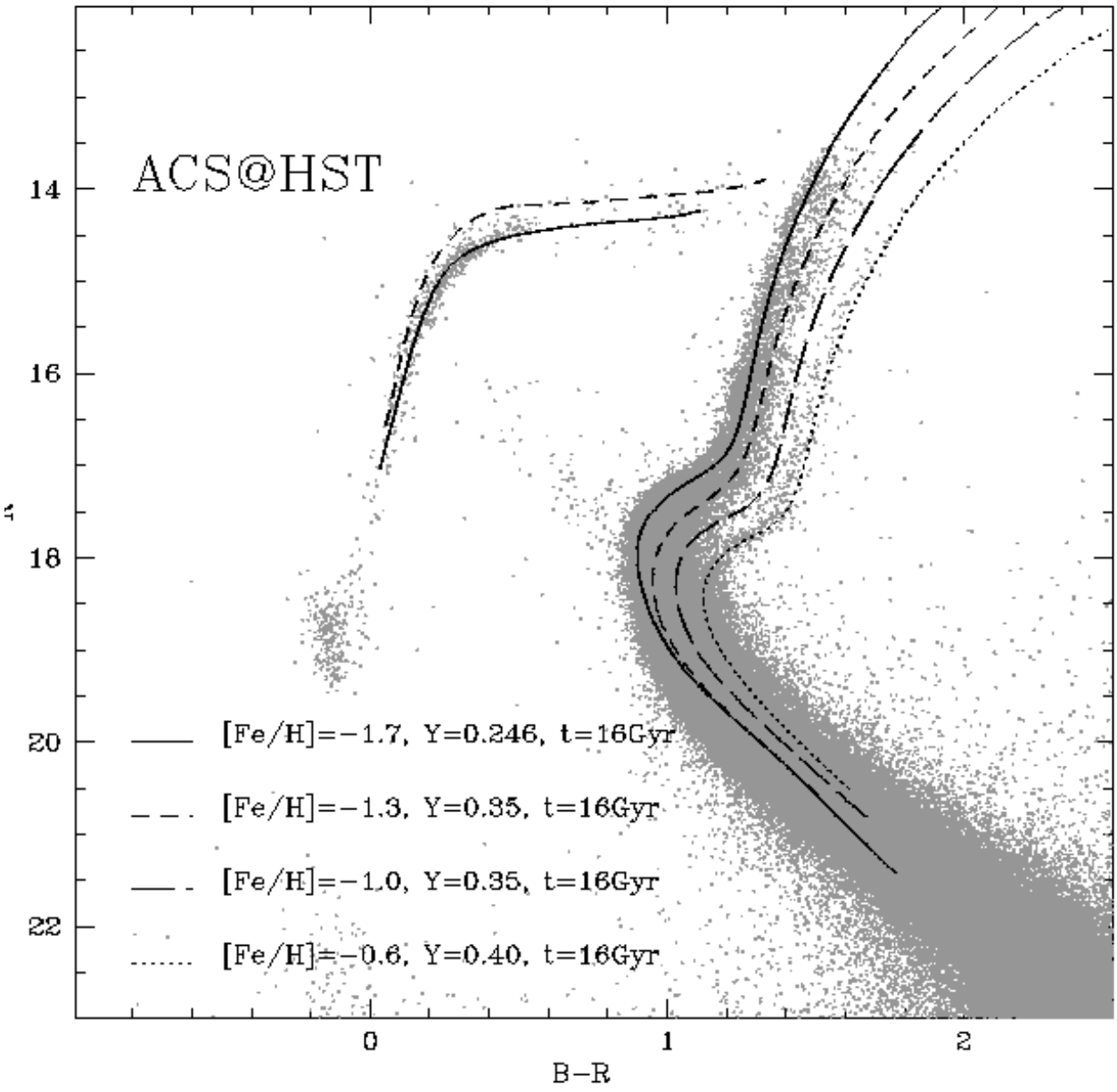

Fig. 8.— ACS CMD of ω Cen. Theoretical isochrones with the bestfit parameters indicated in §4.2 are overplotted.

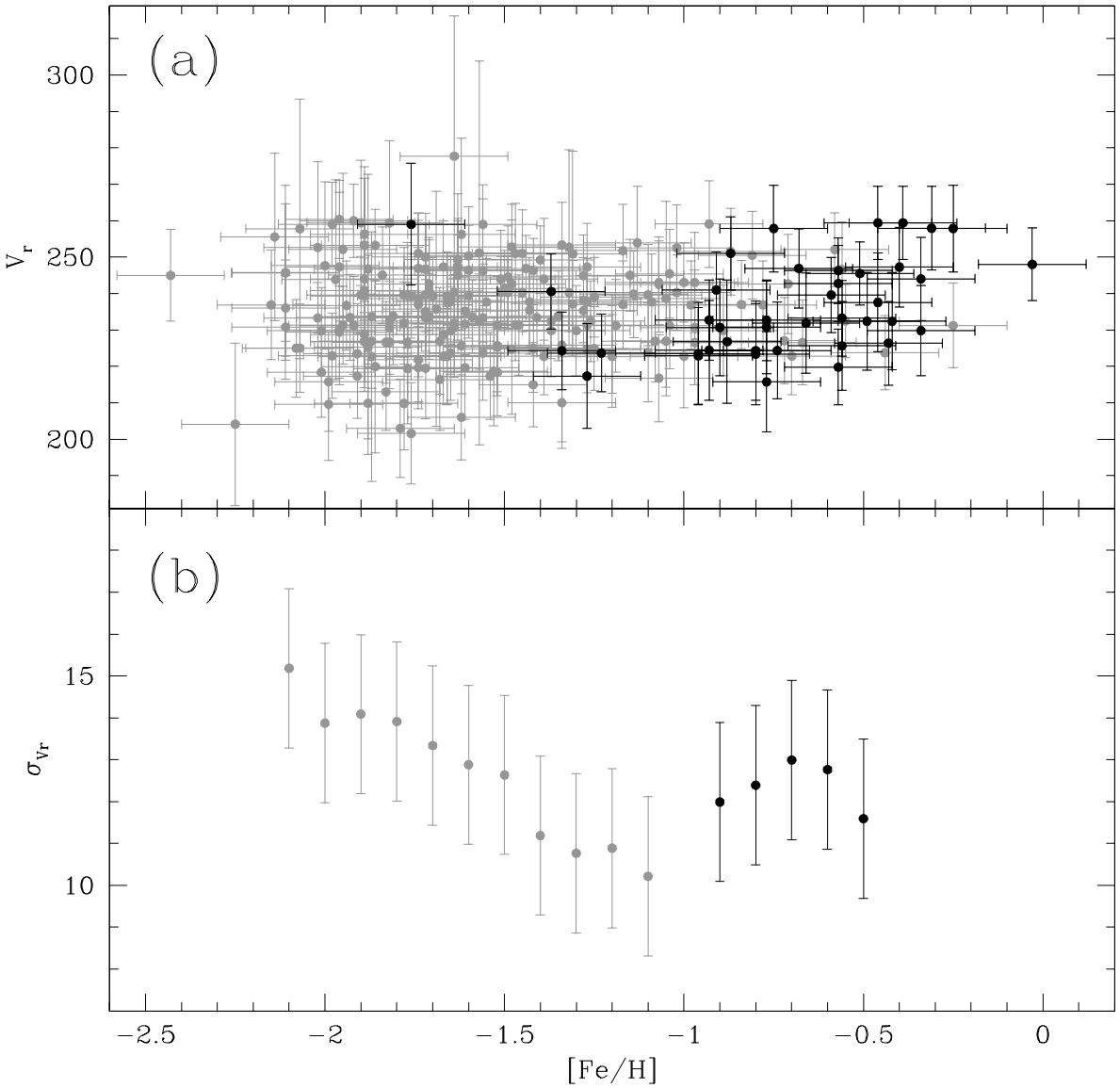

Fig. 9.— Radial velocity as a function of metallicity (*panel* a). The velocity dispersion is plotted against metallicity in *panel* b. SGB-a stars are marked in both panels with black symbols.

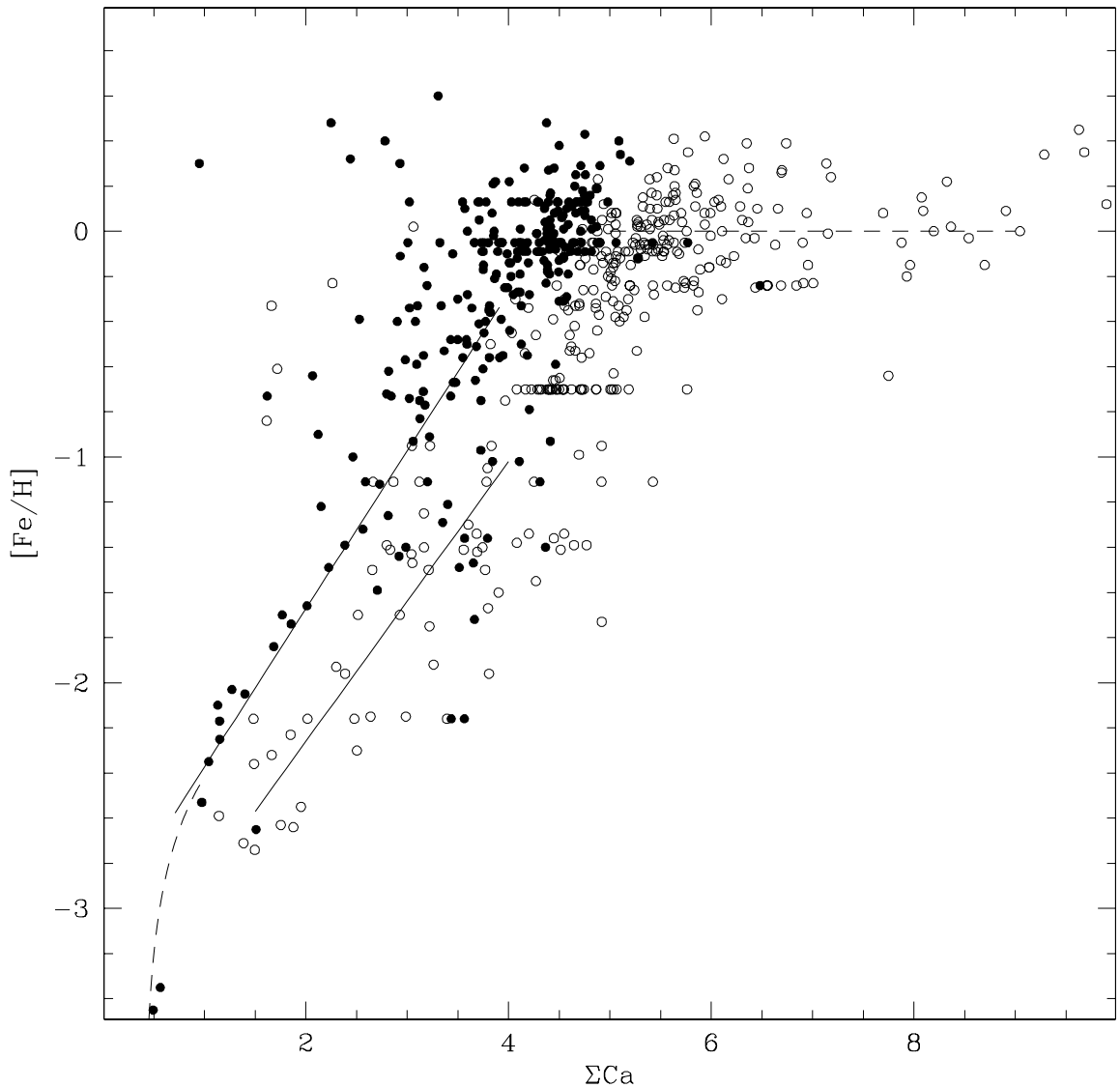

Fig. 10.— Metallicity dependence of the $\Sigma\ Ca$ index for the 603 stars of C01. Open points indicate stars with $log\ g < 3$, filled points indicate stars with $log\ g > 3$. The linear behaviour of the $\Sigma\ Ca$ index as a function of metallicity is indicated with solid lines. Dashed lines represent the behaviour of the $\Sigma\ Ca$ index in the range where it does not correlate linearly with metallicity.

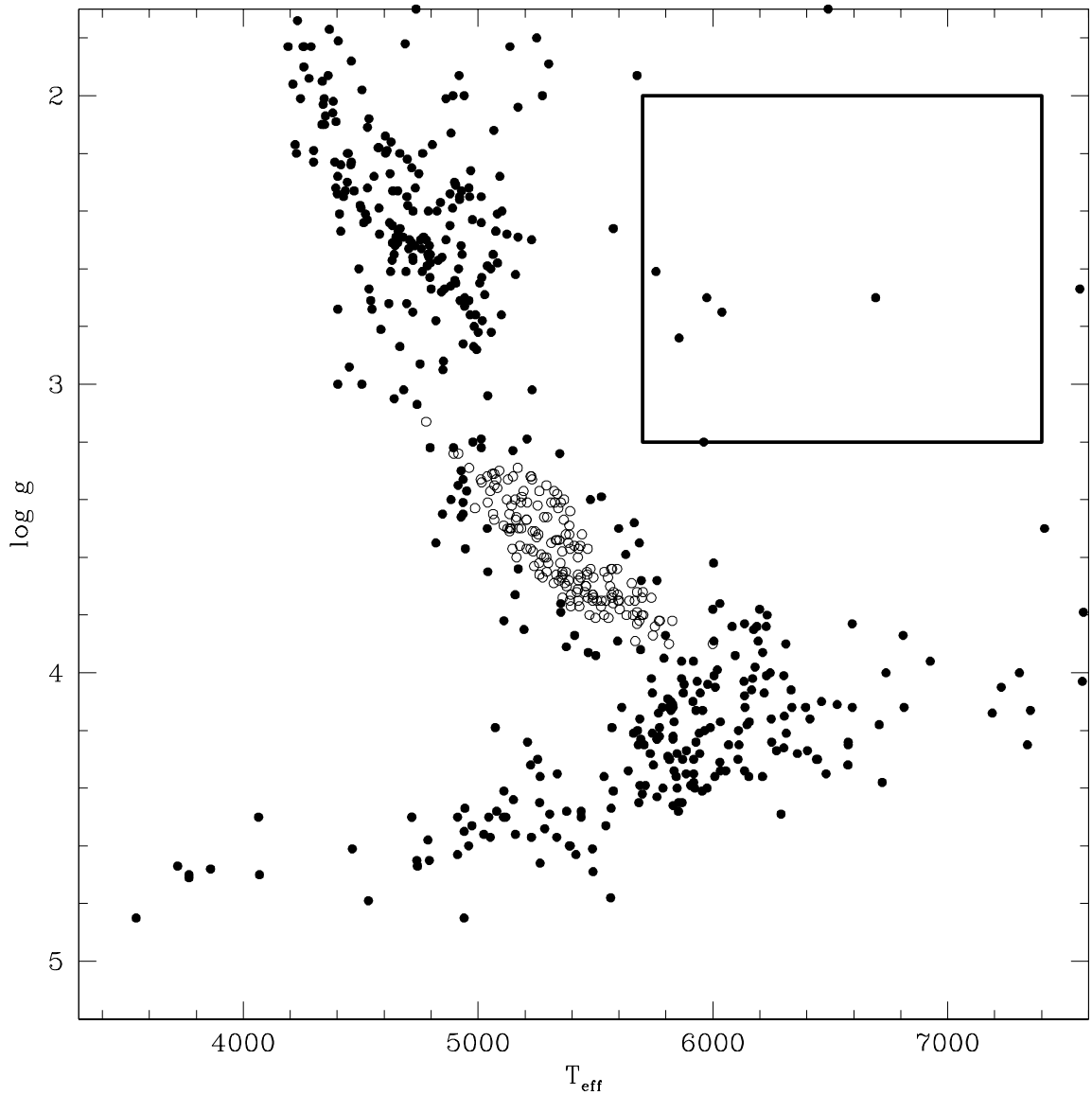

Fig. 11.— $log\ g - T_{eff}$ plane. The calibration stars by C01 (filled circles) and ω Cen target stars (open circles) are shown. The size of the selection box used for the $\Sigma\ Ca - [Fe/H]$ calibration is indicated.

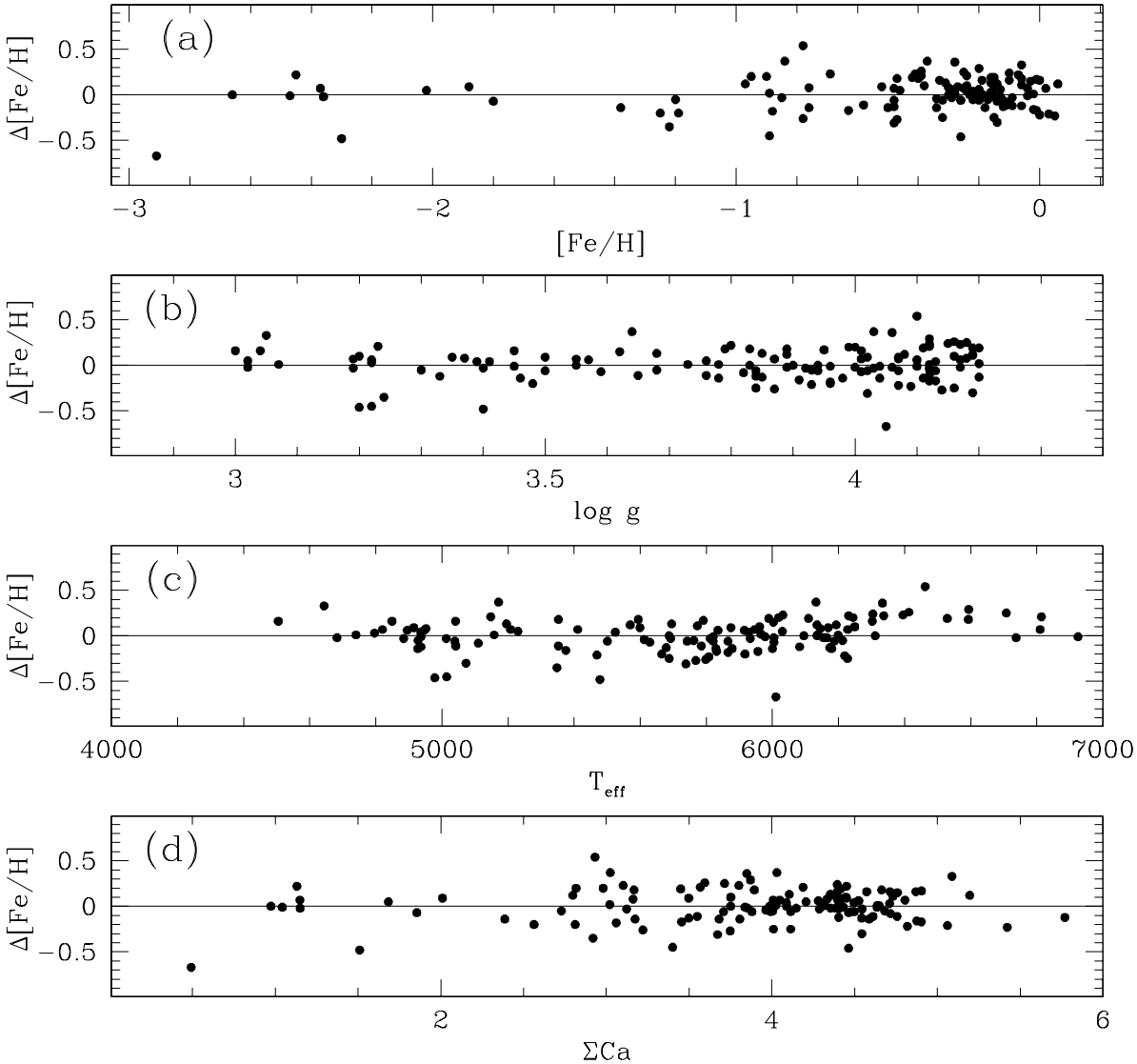

Fig. 12.— Residuals of the metallicity derived following the procedure described in this appendix with respect to the values listed by C01 as a function of [Fe/H] (*panel* a), log g (*panel* b), T_{eff} (*panel* c) and $\Sigma\ Ca$ (*panel* d).

Table 1. Ca II triplet lines and continuum bands

Feature name	Line center ($\AA$)	Line band ($\AA$)	Blue continuum band ($\AA$)	Red continuum band ($\AA$)
λ_{8498}	8498.1	8490 – 8506	8346 – 8489	8563 – 8642
λ_{8542}	8542.3	8532 – 8552	8346 – 8489	8563 – 8642
λ_{8662}	8662.4	8653 – 8671	8563 – 8642	8697 – 8754

Table 2. The populations of ω Cen

Population	[Fe/H]	[α/Fe]	Y	Δ Age (Gyr)
MP	-1.7	0.3	0.246	0
MInt2	-1.3	0.3	0.246	0
MInt2	-1.3	0.3	0.30	0
MInt2	-1.3	0.3	0.35	0
MInt3	-1.0	0.3	0.246	1
MInt3	-1.0	0.3	0.30	1
MInt3	-1.0	0.3	0.35	0
a	-0.6	0.1	0.246	>1
a	-0.6	0.1	0.30	$0 \div 1$
a	-0.6	0.1	0.35	$0 \div 1$
a	-0.6	0.1	0.40	0